

A086732

4224 / (9) Memorandum v. pt.

SECURITY CLASSIFICATION OF THIS PAGE (When Data Entered)

REPORT DOCUMENTATION PAGE		READ INSTRUCTIONS BEFORE COMPLETING FORM
1. REPORT NUMBER NRL Memorandum Report 4220	2. GOVT ACCESSION NO. AD-A086 732	3. RECIPIENT'S CATALOG NUMBER 111
4. TITLE (and Subtitle) EXPERIMENTS ON THE INJECTION OF RELATIVISTIC ELECTRON BEAMS INTO PREFORMED CHANNELS IN THE ATMOSPHERE: A FEASIBILITY STUDY.	5. TYPE OF REPORT & PERIOD COVERED Interim report on a continuing NRL problem.	
	6. PERFORMING ORG. REPORT NUMBER	
7. AUTHOR(s) M. Raleigh, J.D. Sethian, R.B. Florito, L. Allen, R.F. Fernster, and J.R. Greig	8. CONTRACT OR GRANT NUMBER(s) 116 RB011091 117 RB0110901	
9. PERFORMING ORGANIZATION NAME AND ADDRESS Naval Research Laboratory Washington, D.C. 20376	10. PROGRAM ELEMENT, PROJECT, TASK AREA & WORK UNIT NUMBERS 61153N; R011-09-41; 67-0871-0-0	
11. CONTROLLING OFFICE NAME AND ADDRESS Office of Naval Research Arlington, Va. 22217	12. REPORT DATE May 13, 1980	
	13. NUMBER OF PAGES 48	
14. MONITORING AGENCY NAME & ADDRESS (if different from Controlling Office) AD-EMPD 052	15. SECURITY CLASS. (of this report) UNCLASSIFIED	
	15a. DECLASSIFICATION/DOWNGRADING SCHEDULE	
16. DISTRIBUTION STATEMENT (of this Report) Approved for public release; distribution unlimited.		
17. DISTRIBUTION STATEMENT (of the abstract entered in Block 20, if different from Report)		
18. SUPPLEMENTARY NOTES *Permanent address: Naval Surface Weapon Center, White Oak, Md. †Permanent address: JAYCOR, Alexandria, Va. 22304 Work performed at the Naval Research Laboratory under the auspices of the Office of Naval Research.		
19. KEY WORDS (Continue on reverse side if necessary and identify by block number) Relativistic electron beam Channel Atmosphere		
20. ABSTRACT (Continue on reverse side if necessary and identify by block number) Reduced-density channels were created by designating a path through the atmosphere by laser-induced, aerosol-initiated air-breakdown, and heating the air along the path with a guided electric discharge. A Nd: glass laser (~ 60J, ~ 40 nsec), focussed with a 5 m f.l. lens, was used and air-breakdown was enhanced by the presence of a light smoke. The electric discharge (240 kV, ~ 10kA peak current, period ~ 8 μsec) followed the laser path and damped in ~ 6 μsec; ~ 30 μsec later a hot, reduced density, partially ionized channel had formed. The diameter of the channel was ~ 2.0 cm and channels of length up to 2 m have been produced. (Continues)		

251250

## 20. Abstract (Continued)

Using a field emission diode with a  $43 \mu\text{m}$  titanium foil anode, an intense relativistic electron beam ( $\sim 27 \text{ nsec}$ ,  $\sim 2.4 \text{ kA}$ ,  $\sim 1.0 \text{ MeV}$ ) was produced which could be seen propagating in the unperturbed atmosphere for distances  $\sim 100 \text{ cm}$ . This beam was injected into the preformed channel within  $\sim 3 \text{ cm}$  from the anode foil to study the beam-channel interaction. Conditions in the channel were varied by controlling the time between creation of the channel and injection of the REB. When injected into a conducting channel with density  $\sim 6 \times 10^{-5} \text{ g/cm}^3$ , and  $n_e \sim 10^{14} \text{ cm}^{-3}$ , the beam expanded and was ejected from the channel within  $\sim 10 \text{ cm}$  of travel. But when injected into a channel with much lower conductivity and density  $\sim 3 \times 10^{-4} \text{ g/cm}^3$  the beam propagated in the channel and the effect of the reduced scattering was observed.

Analysis of these results shows that they are consistent with accepted theory of beam-plasma interactions, and that the ejection of the REB from the conducting channel was caused by a "self-hose"-like instability.

TABLE OF CONTENTS

I. INTRODUCTION . . . . . 1

II. PRODUCTION OF HOT, REDUCED-DENSITY CHANNELS IN THE  
ATMOSPHERE . . . . . 3

III. PRODUCTION OF AN INTENSE RELATIVISTIC ELECTRON BEAM. 6  
 a) The Pulse Generator and the Diode . . . . . 6  
 b) The Intense REB and the Beam Diagnostics . . . . . 7

IV. INJECTION OF AN INTENSE REB INTO A PREFORMED  
CHANNEL . . . . . 10

V. DISCUSSION . . . . . 13

VI. CONCLUSIONS . . . . . 24

VII. ACKNOWLEDGEMENTS . . . . . 25

VIII. REFERENCES . . . . . 30

**S** DTIC  
 ELECTE **D**  
 JUL 16 1980  
**B**

ACCESSION for		
NTIS	White Section	<input checked="" type="checkbox"/>
DDC	Buff Section	<input type="checkbox"/>
UNANNOUNCED <input type="checkbox"/>		
JUSTIFICATION _____		
BY _____		
DISTRIBUTION/AVAILABILITY CODES		
Dist.	AVAIL.	and/or SPECIAL
<b>A</b>		

Experiments on the Injection of Relativistic  
Electron Beams into Preformed Channels in the Atmosphere  
A Feasibility Study

I. INTRODUCTION

When an intense charged particle beam passes through a gaseous atmosphere it creates a hot, ionized channel along the beam path<sup>1</sup>. It is the interaction of the beam with this channel that determines the beam expansion, stability, and propagation.<sup>2</sup> In pellet fusion<sup>3</sup> where a high density gas blanket is advantageous, loss of beam particles because of scattering in the gas atmosphere can be significant especially for light ion beams. Then it becomes desirable to create a reduced-density, ionized, current-carrying channel through the gas atmosphere in which to propagate the charged particle beam.<sup>4,5</sup>

We report initial results of <sup>was made</sup> a study of the interaction of an intense relativistic electron beam (REB) with a preformed reduced density channel in the atmosphere. The channel was designated by laser-induced, aerosol-initiated air-breakdown and was heated by passage of an electric current.<sup>7</sup> However, at the time the REB was injected into the channel no externally applied heating current remained. By varying the time between creation of the hot channel and injection of the REB, we were able to observe interactions of the beam with both high conductivity and low conductivity channels. In the former case the beam did not propagate in the channel, whereas in the latter case the beam did propagate in the

Manuscript submitted March 5, 1980

channel. These results are discussed in terms of the residual conductivity in the channel, and in terms of the radius of the return current distribution compared to that of the beam.

## II. PRODUCTION OF HOT REDUCED DENSITY CHANNELS IN THE ATMOSPHERE

In recent experiments<sup>4,5</sup> intense relativistic electron beams for pellet fusion studies have been transported along current carrying plasma channels produced by z-pinch discharges and wire-guided discharges. While it was suggested some time ago that lasers might be used to create such plasma channels<sup>8</sup> the demonstration of suitable laser-produced channels came only recently.<sup>6,7</sup> For the present experiments the path of the channel through the atmosphere was designated by laser-induced, aerosol-initiated air-breakdown<sup>9</sup> using a Q-switched Nd:glass laser.<sup>10</sup> The laser radiation ( $\sim 60$  J in  $\sim 40 \times 10^{-9}$  sec) was focused with a 5m focal length lens (Fig. 1) and air-breakdown was enhanced by the presence of a light smoke produced by the combustion of  $\sim 2.5$  gm of black powder. The resultant aerosol density was  $< 10^{-7}$  gm/cm<sup>3</sup> ( $\sim 10^{-2}\%$  by weight in the atmosphere) and the particle size was such that a useable smoke remained in suspension for  $\sim 1$  hour.

The diameter of the laser beam at the focusing lens was  $\sim 5$  cm so that for channels of length  $< 2$ m symmetrically placed about the focus of the lens, the maximum diameter of the laser beam over the channel length was  $< 1$  cm. Within this diameter the aerosol initiated air-breakdown produced randomly spaced plasma beads (Figs. 2 and 3b) and sufficiently perturbed conditions in the atmosphere to guide an electric

discharge along the laser path provided the voltage was applied between 10 and 100  $\mu\text{sec}$  after the Nd:glass laser had been fired.

The electric discharge for heating the laser designated channel was provided by a small Marx generator ( $V_{\text{max}} \approx 360$  kV,  $C \approx .015 \mu\text{F}$ ,  $R_{\text{int}} \approx 4.5 \Omega$ ,  $L_{\text{int}} \approx 6 \mu\text{H}$ ) which was normally charged to  $\approx 240$  kV and fired  $\approx 30 \mu\text{sec}$  after the Nd:glass laser. The current and voltage for a typical 50 cm long laser guided discharge are shown in Fig. 4. From an analysis of the circuit parameters<sup>7</sup> it was deduced that  $\approx 3.5$  J/cm were deposited in the channel.

The diameter of the discharge-heated channel was obtained by both open shutter and Schlieren photography (Fig. 3). With the latter technique the expansion and subsequent cooling of the channel was also followed (Fig. 5). From such records it was estimated that the radius of the discharge-heated channel was 2.5 mm so that the electrical energy deposited in the channel was  $\approx 18$  J/cm<sup>3</sup>. The hot channel subsequently expanded reaching atmospheric pressure when the diameter was  $\approx 2.2$  cm, which corresponds to a volume expansion ratio of  $\approx 20$ . From this we calculated that the temperature of the expanded channel was  $\approx 5000$  K and there was  $\approx 20\%$  dissociation. Assuming the expansion was adiabatic with a mean specific heat ratio<sup>11</sup> of  $\gamma \approx 1.2$ , we estimated that the temperature of the hot channel before expansion was  $\approx 7500$  K and the internal energy<sup>11,12</sup>

was  $\approx 18 \text{ J/cm}^3$  in agreement with the measured electrical energy deposition.

Thus between 35 and 100  $\mu\text{sec}$  after initiation of the heating current pulse, long straight channels (Fig. 6) have been formed which have a diameter of  $\approx 2 \text{ cm}$ , a mass density  $\approx 1/20$  that of the normal atmosphere, and a free electron density<sup>12,13</sup> of  $\approx 10^{14} \text{ cm}^{-3}$ . In the next several milliseconds these channels cooled by turbulent entrainment of cold air from the surrounding atmosphere (Fig. 5). The temperature during this cooling was estimated<sup>7</sup> by assuming that the air in the hot channel mixed uniformly with the cold air around it, conserving energy and expanding to maintain atmospheric pressure. Then starting at a temperature of  $\approx 5000 \text{ K}$  and density  $\approx 6.5 \times 10^{-5} \text{ gm/cm}^3$  the channel cooled and expanded as shown in Table 1.

### III. PRODUCTION OF AN INTENSE RELATIVISTIC ELECTRON BEAM

#### III. a). The Pulse Generator and the Diode

The relativistic electron beam was produced by a modified Physics International Pulserad 310 accelerator, consisting of a 10 stage oil-insulated Marx generator driving a 40 ohm oil dielectric Blumlein terminated with a cold-cathode field emission diode. Each stage of the Marx generator contained one .1 $\mu$ f at 100 kV capacitor for a total stored Marx energy of 5.0 kJ. Power was switched to the Blumlein through a self-break oil switch and under ideal conditions, the shot-to-shot jitter from trigger to the Marx to beam firing could be made less than  $\pm 20$  nsec. The diode assembly was a 1.2 cm radius annular carbon cathode (.63 cm annular width) separated by 1.5 cm from a .043 mm thick titanium foil anode.

Typically, the electron beam characteristics inside the diode were  $V = 940$  kV,  $I = 24$  kA, with a pulse width of 27 nsec F.W.H.M. As the anode foil was usually ruptured after each shot, an appropriate foil holder was fabricated to allow rapid replacement of the anode. Using two such holders, the time between shots was limited only to that necessary to evacuate the diode to a base pressure of less than  $10^{-4}$  torr, typically 20 minutes. The accelerator could be fired 10-15 times before a complete cleaning of the diode internal surfaces and a redressing of the cathode were necessary.

### III. b). The Intense REB and the Beam Diagnostics

To produce a "stable" relativistic electron beam the output from the diode was restricted by a carbon block  $\approx$  11 cm diameter by 1 cm thick with a 1.5 cm diameter hole at its center (Fig. 7). The center of the carbon block was  $\approx$  3 cm from the anode foil. Of the  $\approx$  24 kA of current inside the diode, only  $\approx$  8 kA emerged through the anode foil and of this, only  $\approx$  2.4 kA came through the hole in the carbon block. Current measurements were made with a B-dot loop inside the diode and Rogowski coils outside the diode. These different devices were calibrated to  $\pm 10\%$  for currents with these time variations. The plasma return current ( $I_p$ ) flowing back to the anode foil was estimated by comparing currents measured on a Rogowski coil and a carbon calorimeter and was found to be less than the 10% uncertainty in the net current ( $I_N$ ).

A qualitative study of the beam current distribution across the anode foil was made using a thin film dosimeter<sup>14</sup> (blue cellophane). The emission consisted of a peak of current density at the center of the anode foil containing  $\approx$  1 kA in a circle of area  $\approx$  0.1 cm<sup>2</sup> surrounded by a halo about 1 cm<sup>2</sup> in area containing another  $\approx$  2 kA. The remainder of the beam current ( $\approx$  5 kA) was spread over  $\approx$  10 cm<sup>2</sup> of anode area with current density near the threshold of detection ( $\approx$  0.5 kA/cm<sup>2</sup>). After passing through the aperture in the carbon block the current distribution was more uniform with only a small peak on axis.

To monitor the propagation of the REB through the atmosphere several different diagnostics were used. These are shown schematically in Fig. 8. An open shutter camera (OSC) was used to photograph the path of the REB in visible light. This camera was wrapped in  $\sim$  3 mm thick, lead sheet and viewed the beam path through a front surfaced mirror as indicated. A typical photograph of the freely propagating beam is shown in Fig. 7.

One Rogowski coil (RC 1) was placed next to the carbon block to measure the net current at injection. A second Rogowski coil (RC 2) which is  $\sim$  30 cm diameter was placed 25 cm from the carbon block to measure the downstream current. A tungsten grid (TG) consisting of  $\sim$  1.6 mm diameter tungsten wires spaced  $\sim$  5 mm apart over an area 14 cm by 13 cm was used to show the position and size of the REB. This grid was placed at  $\sim$  45 $^\circ$  to the direction of the beam, 50 cm from the carbon block, and was photographed with an x-ray pinhole camera (XPC 1). Closer to the carbon block was a 30 cm by 30 cm sheet of polycarbonate (Lexan). This sheet (LP in Fig. 8) was  $\sim$  1.5 mm thick and had a 2.5 cm diameter hole at its center. It was inclined at  $\sim$  45 $^\circ$  to the direction of the REB with the hole  $\sim$  10 cm from the carbon block. The polycarbonate sheet was photographed by a second x-ray pinhole camera (XPC 2) to determine the radial position of the REB at  $\sim$  10 cm.

Typical data for the freely propagating beam are shown in Figs 9a, 10a, and 11a and in Table 2. The peak net injected current was  $\approx 2.4$  kA as measured on RC 1, and without the Lexan plate (LP in Fig. 8) this full current was measured up to 50 cm from the carbon block using RC 2. In the unperturbed atmosphere the hole in the Lexan plate was easily aligned with the REB and a reproducible 60% of the injected current ( $\approx 1.45$  kA, passed through the hole, (measured on RC 2). The x-ray image of the tungsten grid at 50 cm was not so reproducible (see Figs. 9a, 10a, and 11a) but a clearly defined image was always seen even with the Lexan plate in position. The diameter of this image was  $\approx 9$  cm (Fig. 11a).

#### IV. INJECTION OF AN INTENSE REB INTO A PREFORMED CHANNEL

To allow the intense REB to be injected into a preformed channel, the laser-designated, electric-discharge-heated channel described in Section II was established along the path of the electron beam. This was achieved as shown in Fig. 12, using the tungsten grid (TG) as the high voltage electrode and the carbon block (C) as the ground electrode. In initial attempts to form the hot channel in front of the diode, the Nd:glass laser radiation punctured the titanium anode foil (A). To prevent this the foil assembly (FA) was installed in front of the carbon block (C). The foil assembly consisted of six aluminized Mylar foils stretched on lucite frames with  $\approx 4$  cm diameter apertures in them. The foils were held at a small angle ( $\lesssim 10^\circ$ ) so that the reflected laser radiation did not return to the laser. As the Mylar foils were only  $\approx 6$   $\mu\text{m}$  thick the Nd:glass laser alone usually burst the first 4 foils. The electric discharge then destroyed and evaporated the remaining foils, leaving a clear aperture of  $\approx 3$  cm diameter through the whole assembly. In Section III, the typical data for the freely propagating REB were taken with the foil assembly in place but without the Nd:glass laser or the electric discharge. Passage of the REB through the Mylar foils did not damage the foils. The presence of the foils either cold or evaporated by the laser alone did not affect the net current measured on RC 1 or RC 2.

To inject the REB into the preformed channel the Nd:glass laser was fired first to designate the channel path, 30  $\mu$ s later the Marx generator was fired to heat the channel, then after a chosen delay ( $\tau$ ) the electron beam generator was fired. The passage of the REB along the channel was monitored with the same set of diagnostics as for the freely propagating beam (Fig. 8), with the tungsten grid still 50 cm from the carbon block. Typical results are shown in Figs. 9, 10, and 11 and in Table 2 for  $\tau = 100 \mu$ s and  $\tau = 500 \mu$ s.

At  $\tau = 100 \mu$ s the peak net current injected into the channel was only  $\sim 2.1$  kA (Table 2) even though the diode characteristics were not visibly affected by the presence of the laser guided discharge. In  $\sim 50\%$  of these shots the REB was ejected from the preformed channel within a few centimeters of travel from the carbon block and struck the Lexan plate (Figs. 9b and c and 10b). Then only  $\sim 30\%$  of the net injected current ( $\sim 0.63$  kA) was measured on the second Rogowski coil (RC 2). The beam appeared to expand out of the channel and be deflected from it, though the expansion was not uniform, (Figs. 9 and 10). In the other 50% of the shots when  $\sim 60\%$  of the injected current ( $\sim 1.3$  kA) went through the Lexan plate and when the Lexan plate was removed (in which case 100% of the injected current passed through the second Rogowski coil), the x-ray image of the tungsten grid at 50 cm was never more than weak (Figs. 9c, 10b, and 11b and c). Occasionally with  $\tau = 100\mu$ s the x-ray image recorded in XPC 1 filled the field of view of the camera (Fig.

9b) suggesting that the image was produced by beam electrons being "sprayed" on the camera itself.

At  $\tau = 500 \mu\text{s}$  the peak net current injected into the channel was the same as that injected into the unperturbed atmosphere (Table 2). Also, a reproducible  $\sim 60\%$  of the net injected current passed through the hole in the Lexan plate. However the x-ray image of the tungsten grid at 50 cm was always much brighter and sharper than that seen in the unperturbed atmosphere (Figs. 10c and 11d). The diameter of this image was  $\sim 4$  cm (Fig. 11d).

Similar results were obtained when the channel length was increased to 100 cm by moving the tungsten grid to be 100 cm from the carbon block.

## V. DISCUSSION

Following the deposition of electrical energy in the air by the laser guided discharge, the hot air channel expanded to a radius of  $\approx 1$  cm. Thus at the end of the channel where the current passed into the carbon block there must have been an axial expansion comparable to, but smaller than the radial expansion, i.e.  $\Delta z < 1$  cm. This expansion is about equal to the thickness of the carbon block and indicates that the hot channel did not spread into the gap of 2.5 cm between the carbon block and the anode foil. Therefore the presence of the hot air channel should not have changed the situation existing between the carbon block and the anode foil, and the REB injected into the hot air channel should have been the same as that injected into the unperturbed atmosphere, i.e. in both cases  $I_b \approx 2.4$  kA.

The position of the carbon block (C in Fig. 7) was chosen to maximize the current passing through the 1.5 cm diameter aperture in the block. This corresponded to placing the carbon block at the first "pinch point" in the beam coming out of the anode foil. [The first and second pinch points in the beam were easily seen using the thin film dosimeter (blue cellophane).] As indicated in §IIIb the distribution of current density across the anode foil consisted

of a sharp peak at the center of the foil ( $\sim 1$  kA) with wings spreading out to a radius of  $\sim 2$  cm. The mean square scattering angle introduced by the anode foil<sup>15</sup> was

$$\langle \theta^2 \rangle_{\text{foil}} \sim 0.17 \text{ radian}^2$$

and for electrons emanating from the center of the anode foil only those with

$$\theta < 0.2 \text{ radian}$$

passed through the aperture in the carbon block. However the dimensions of the aperture allowed

$$\theta \lesssim 1 \text{ radian}$$

and the pinching of the electron beam caused

$$\theta_{\text{max}} \sim r_{\text{max}} \omega_{\beta} \sim 0.6 \text{ radian}$$

where  $\omega_{\beta} = \sqrt{2e\beta I_N / \gamma mc} / r$  is the Betatron frequency and  $r$  is the beam radius. Therefore the mean square scattering angle for the electron beam emerging from the aperture in the carbon block must have been approximately that produced by the anode foil, and the beam must have been overpressure by

$$\frac{kT_{\perp}}{kT_B} \sim 2,$$

where  $T_B$  is the Bennett temperature<sup>16</sup>, i.e. that necessary for the beam to have been in pressure equilibrium.

Assuming it expands against its own magnetic field, the beam will have expanded to reach pressure equilibrium at radius

$$a \approx 1.25 \text{ cm}$$

while travelling an axial distance of approximately

$$z \approx 2 \text{ cm.}$$

In the following analysis we assume that the electron beam can be represented by a Bennett profile<sup>17</sup>,

$$J_b(r) = \frac{I_b}{\pi a^2 \left(1 + (r/a)^2\right)^2} \quad 1$$

where  $J_b(r)$  is the current density at radius  $r$  and  $a$  is the Bennett radius. Then for

$$z > 2 \text{ cm}$$

and for the beam propagating in the unperturbed atmosphere

$$\omega_B \approx 3 \frac{\epsilon_\gamma}{T_B}$$

where  $\epsilon_\gamma$  is the rate of increase of transverse kinetic energy per electron due to scattering on air molecules.<sup>15</sup> Thus the beam was a pinched, matched beam as suggested by the photograph shown in Fig. 7 and expanded according to the Nordsieck equation<sup>17</sup>

$$\frac{d}{dt} \left( \ln \left( \frac{a(t)}{a(0)} \right)^2 \right) = \frac{\epsilon_\gamma}{T_B} \quad 2$$

Using this equation we calculate the beam radius at

$$z = 50 \text{ cm}$$

as

$$a(50) \approx 10 \text{ cm},$$

though the Nordsieck equation is only marginally applicable for such large beam radii. Thus the diameter of the electron beam (full width at half maximum intensity) as it struck the tungsten grid was  $\approx 13$  cm which is in reasonable agreement with the x-ray photograph shown in Fig. 11a.

With the Lexan plate in place (LP in Fig. 8) at  $z = 10$  cm, the beam radius was already as large as or bigger than the hole in the plate. Therefore if the beam profile had been a true Bennett profile (at  $z = 10$  cm),  $\approx 50\%$  of the beam would have been stopped by the plate. In practice  $\approx 62\%$  of the beam passed through the hole in the Lexan plate and was measured on the second Rogowski coil. When this reduced electron beam propagated in the unperturbed atmosphere, it first expanded again to reach a new Bennett equilibrium, then

$$\omega_{\beta} \approx \frac{eY}{T_B}$$

but again using the Nordsieck expansion

$$a(50) \approx 27 \text{ cm}.$$

This radius is rather large compared to that seen in the x-ray photographs in Figs. 9a and 10a, but this may be due to the non-Bennett nature of the current distribution, or perhaps to a secondary pinching effect produced by the Lexan plate. Values of  $a(50)$  are collected in Table 3 for easy comparison.

In considering the interaction of the REB with the atmosphere plus the hot channel the first question to ask is whether the channel produced by the laser guided discharge caused a significant change in the conductivity along the path of the electron beam. The rate of production of plasma electrons in the atmosphere is given by<sup>18</sup>

$$\dot{n}_e(r) = \frac{1}{E} \frac{dE}{dz} \frac{J_b(r)}{e} - \alpha n_e(r) n_0^2 - \beta n_e^2(r) . \quad 3$$

Here  $\dot{E}$  is  $\sim 33$  eV per ion/electron pair and  $dE/dz$  is the energy loss by a beam electron [ $dE/dz \sim 7 \times 10^{-17} n_0$  eV/cm for  $E \sim 10^6$  volts] so that the first term on the right represents the rate of production of secondary electrons by beam electrons. The second and third terms represent the loss of plasma electrons by three body attachment and dissociative recombination respectively with

$$\alpha \sim 6 \times 10^{-32} \text{ cm}^6 \text{ sec}^{-1}$$

so that  $n_0$  is the total density of air molecules (oxygen plus nitrogen), and

$$\beta \sim 5 \times 10^{-8} \text{ cm}^3 \text{ sec}^{-1}$$

which assumes a plasma electron temperature,  $kT_e \sim 0.5$  eV.

In air at atmospheric pressure dissociative recombination is the dominant loss mechanism so that

$$n_e(t, r) = n_e(\infty, r) \frac{[1 - \exp(-t/\tau_r)]}{[1 + \exp(-t/\tau_r)]} \quad 4$$

where

$$n_e(\infty, r) = \left[ \frac{1}{\beta \tilde{E}} \cdot \frac{dE}{dz} \cdot \frac{J_b(r)}{e} \right]^{1/2} \quad 5$$

and

$$\tau_r = \left[ 2 \left[ \frac{\beta}{\tilde{E}} \cdot \frac{dE}{dz} \cdot \frac{J_b(r)}{e} \right]^{1/2} \right]^{-1} \quad 6$$

The plasma return current density is given by

$$J_p(r) = \sigma(r) E_z(r)$$

where  $E_z(r)$  is the axial electric field at radius  $r$  and  $\sigma(r)$  is the conductivity,

$$\sigma(r) = \frac{n_e(r) e^2}{2m n_0 \sigma_c v_{th}}$$

The collision cross-section  $\sigma_c$  was taken<sup>19</sup> as  $\sim 10^{-15} \text{ cm}^2$  and the mean thermal velocity  $v_{th}$  as  $\sim 5 \times 10^7 \text{ cm/sec}$ .

Then since the variation of  $E_z(r)$  with  $r$  is negligible for  $r \ll a$  and  $R \gg a$ , where  $R$  is the radius of the screened room into which the beam was fired, the total plasma return current is

$$I_p = E_z \int_0^{\infty} 2\pi r \sigma(r) dr \\ = \sum E_z$$

Values of the conductance  $\Sigma$  were calculated for unperturbed air and air with the hot channel at  $\tau \approx 100 \mu\text{sec}$  using  $t \approx 10^{-8}$  sec to represent the mid-point of the current pulse. These values are shown in Table 4. To simplify the calculations the current pulse was assumed to be rectangular. From Table 4 it is clear that the conductance  $\Sigma$  is a strong function of the beam radius ( $a$ ) and for  $a \geq 2$  cm the beam induced conductivity was so small that  $\Sigma$  was dominated by the residual electron density in the hot channel,

$$n_e (\tau \approx 100 \mu\text{sec}) \approx 10^{14} \text{ cm}^{-3}.$$

In these calculations ohmic heating and electric field induced conductivity have been ignored because although

$$E_r \approx \frac{2 I_b (r)}{r}$$

rose above 30kV/cm for  $r < 2$ cm, this field was rapidly minimized by the establishment of charge neutrality (in times  $< 10^{-9}$  sec), and inductive fields were always below breakdown values.

Clearly the residual electron density in the hot channel at  $\tau = 100 \mu\text{s}$  provided significant conductivity compared to the beam induced conductivity. Whereas with much lower residual electron density in the channel i.e. for  $\tau = 500 \mu\text{s}$  the conductance  $\Sigma$  was the same as for propagation in the unperturb-

ed atmosphere. Since there was no plasma return current when the REB propagated in the unperturbed atmosphere (§IIIb) the net injected current for the REB propagating in the channel with  $\tau = 500$   $\mu$ s should have been the same as that for propagation in the unperturbed atmosphere and in both cases

$$I_N = I_b .$$

As seen in Table 2, this was the case.

When the generator, acting as a current source, injects the electron beam into the atmosphere with a conducting channel, i.e.  $\tau = 100$   $\mu$ s, the equivalent circuit consists of a beam inductance  $L$  in parallel with the channel resistance  $R$  and channel inductance  $L_c$  which are in series. Then the current source injects the beam current  $I_b$ , the net current  $I_N$  flows in the beam inductance, and the plasma current  $I_p$  flows through the channel. Since the beam current can be reasonably represented by

$$I_b = I_0 \sin \omega t$$

for  $0 < \omega t < \pi$ , where  $I_0 \approx 2.4 \times 10^3$  amp and  $\omega \approx 0.8 \times 10^8$   $\text{sec}^{-1}$ , the net current  $I_N$  is given by

$$I_N = \frac{I_0}{1+\alpha^2} \left( \sin \omega t - \alpha \cos \omega t + \alpha e^{-\omega t/\alpha} \right)$$

where  $\alpha = \omega L/R$  provided  $R \gg \omega L_c$ . Then to reproduce the peak net current of  $2.1 \times 10^3$  amp,  $\alpha \approx 0.6$  and for  $L \approx 340$  nH,  $R \approx$

45  $\Omega$ , which is in good agreement with the conductance calculated for the channel (Table 4). At the same time the peak of the net current should be delayed by  $\sim 11$  ns from the peak of the beam current but no measurement of this delay was made. From the same model the peak plasma return current is  $\sim 1$  kA and should occur at  $\sim 11$  ns into the current pulse.

In the channel at  $\tau = 500 \mu\text{s}$

$$n_0 (\tau = 500 \mu\text{s}) = 1/4 n_0 (\text{unperturbed})$$

therefore  $\epsilon_\gamma (\tau = 500 \mu\text{s}) = 1/4 \epsilon_\gamma (\text{unperturbed})$

and from the Nordsieck equation for the case without the Lexan plate

$$a(50) \sim 2\text{cm}$$

which is in good agreement with the x-ray photograph shown in Fig. 11d. With the Lexan plate in position the beam expanded more (Table 3) but since the REB was then wider than the channel, the x-ray photograph of the tungsten grid should perhaps have a bright center with the same diameter as the channel i.e.  $\sim 2\text{cm}$  and a weaker image around it. This is in reasonable agreement with the photograph shown in Fig. 10d.

When the REB was injected into the hot channel at  $\tau = 100 \mu\text{s}$

$$n_0 (\tau = 100 \mu\text{s}) \sim 1/20 n_0 (\text{unperturbed})$$

therefore if the REB had propagated in this channel even with the reduced net current

$$a(50) \approx 1.6 \text{ cm}$$

without the Lexan plate and this is clearly not substantiated by the results shown in Fig. 11. After emerging from the aperture in the carbon block the REB expanded in this case to

$$a \approx 1.5 \text{ cm}$$

at

$$z \approx 3 \text{ cm}$$

Since the channel radius was  $\approx 1$  cm only a fraction of the beam was actually within the channel,  $\approx 0.75$  kA for a Bennett profile. Therefore with the plasma return current of  $\approx 1$  kA in the channel the magnetic pressure in the channel was a net outward pressure, causing the REB to become hollow. Even without much hollowing the beam was essentially propagating outside the channel in the normal density air and the radius of the beam when it struck the tungsten grid was much larger (Table 3). These values of  $a(50)$  are more compatible with the results shown in Figs. 9, 10, and 11, i.e. no measurable intensity. However, in those experiments where the Lexan plate was used to monitor the radial position of the REB at  $z \approx 10$  cm, it was found that in  $\approx 50\%$  of the shots into a channel at  $\tau = 100 \mu\text{s}$  the REB struck the Lexan plate and only  $\approx 30\%$  of the injected current was measured on the second Rogowski coil (§IV). The result of such behavior can be seen

clearly in Fig. 9b on the left. The REB appears to have split into two components which have been displaced to opposite sides of the channel probably at different times in the life of the beam. Such behavior is compatible with a "self-hose"-like instability where the plasma return current was fixed in the conducting channel and the channel radius was not significantly larger than the beam radius. Simple models using either a centrally peaked or a uniform plasma return current indicate that for initial misalignments of  $> 0.3$  cm between the axes of the conducting channel and the beam, or equivalent asymmetry in the beam, the beam will be ejected from the channel within  $\sim 10$  cm of travel.

## VI. CONCLUSIONS

We have shown that a hot, reduced-density channel<sup>7</sup> through a gaseous atmosphere which is produced by a laser guided discharge<sup>6</sup> can be established in front of an electron beam generator in such a way that the beam is injected into the channel. The effect of the channel on the injected REB depends on the residual conductivity of the channel and the relative size of the channel compared to the beam. For the case where the channel was conducting ( $n_e \approx 10^{14} \text{ cm}^{-2}$ ,  $\sigma \approx 0.2 \text{ mho/cm}$ ) and narrow i.e.  $\tau \approx 100 \text{ } \mu\text{s}$ , the return current established in the channel was within the beam current distribution and produced an anti-pinching force near the beam axis. Small initial misalignments between the REB and the channel, or asymmetries in the beam grew rapidly, causing the beam to leave the channel in a distance of  $\approx 10 \text{ cm}$ , so that the propagation of the REB in the presence of the narrow, conducting channel was much worse than in the unperturbed atmosphere.

At the later time in the life of the channel ( $\tau \approx 500 \text{ } \mu\text{s}$ ), the channel was larger (radius  $\approx 1.5 \text{ cm}$ ) and had no appreciable residual conductivity. Thus when the REB was injected into this channel the plasma return current was the same as with no channel. The only effect observable was the reduced gas scattering caused by the reduced density of the air in the hot channel (Table 2) which caused the brighter, smaller x-ray emission area on the tungsten grid target.

If now a second "focussing" current pulse can be established in the channel just prior to injection of the electron beam and without incurring gross channel instability, this technique will be directly applicable to pellet fusion schemes<sup>3</sup> using either electron beams or light ion beams.

#### VII. ACKNOWLEDGMENTS

We are deeply grateful to Messrs. Evanson, Laikin, and Pfeiffer; without their exceptional efforts these experiments could not have taken place. We are also happy to acknowledge the assistance given by Drs. Goldstein, Lampe, and Pechacek, whose physical insights have helped in the understanding of the results, and Dr. A.E. Robson who was instrumental in bringing this experiment to fruition.

Table 1 - Expansion and Cooling of Laser Designated,  
Electric Discharge Heated Channels in the  
Atmosphere.

<u>Time</u>	<u>Radius</u>	<u>Density</u>	<u>Temp.</u>
35-100	1.1	$6.4 \times 10^{-5}$	5000
300	1.3	$1.38 \times 10^{-4}$	2800
550	1.5	$3.2 \times 10^{-4}$	1200
1000	1.8	$6.5 \times 10^{-4}$	600
$\infty$	---	$1.29 \times 10^{-3}$	300
$\times 10^{-6}$ sec.	cm	gm/cm <sup>3</sup>	K

Time is measured from the initiation of the heating current pulse.

Table 2. Values of Injected Current

Experiment	$I_N$
REB in unperturbed atmosphere	2.4 ± .05
REB in channel $\tau = 100 \mu\text{sec}$	2.1 ± .09
REB in channel $\tau = 500 \mu\text{sec}$	2.4 ± .05

$I_N$  is the average net injected current in kiloamperes measured on the Rogowski coil RC 1 at the peak of the current pulse.

Table 3. Calculated Electron Beam Radii

Experiment	a(z) at z = 50 cm	
	without Lexan plate	with Lexan plate
REB in unperturbed atmosphere	10	27
REB in channel ( $\tau = 100 \mu\text{sec}$ )	1.6 <sup>*</sup> 16 <sup>**</sup>	44 <sup>**</sup>
REB in channel ( $\tau = 500 \mu\text{sec}$ )	2 <sup>***</sup>	3.5 <sup>***</sup>
	cm	cm

\* assuming that the beam propagated within the channel.

\*\* assuming that beam was hollow and propagated along outside of the channel.

\*\*\* ignoring the fact that the channel radius was only  $\sim 1.5$  cm.

Table 4. Values of the Conductance of the Unperturbed Atmosphere and the Atmosphere with the Hot Channel

	a = 1	1.8	5	10 cm
REB in unperturbed atmosphere	$8.9 \times 10^{11}$	$2.4 \times 10^{11}$	$3.4 \times 10^{10}$	$8.2 \times 10^9$
REB in channel ( $\tau = 100 \mu\text{sec}$ )	$1.4 \times 10^{12}$	$8. \times 10^{11}$	$7.10^{11}$	$6.10^{11}$

Values of the conductance  $\Sigma$  ,

$$\Sigma = \int_0^{\infty} 2\pi r \sigma(r) dr$$

calculated at time  $t = 10^{-8}$  sec assuming a rectangular current pulse, with a Bennett profile where  $a$  is the radius of the current density profile,

$$J_b(r) = \frac{I_b}{\pi a^2 \left(1 + \frac{r^2}{a^2}\right)^2}$$

and  $I_b = 2.4 \times 10^3 \text{ A}$ .

#### VIII. REFERENCES

1. D.A. McArthur and J.W. Poukey, Phys. of Fluids 16, 1996-2004 (1973).
2. E. Lauer, R.J. Briggs, T.J. Fessenden, R.E. Hester, and Edward P. Lee, Phys. of Fluids 21, 1344-52 (1978).
3. G. Yonas, Sci. Amer. 239(5), 50-61 (1978).
4. J. Benford, J. Appl. Phys. 48, 2320-2323 (1977).
5. P.A. Miller, R.F. Butler, M. Cowan, J.R. Freeman, J.W. Poukey, T.P. Wright, and G. Yonas, Phys Rev. Lett. 39, 92-94 (1977).
6. J.R. Greig, D.W. Koopman, R.F. Fernsler, R.E. Pechacek, T.M. Vitkovitsky, and A.W. Ali, Phys. Rev. Lett. 41, 174-177 (1978).
7. M. Raleigh, J.R. Greig, and R.E. Pechacek, Bull. Am. Phys. Soc. 24, 978 (1979).
8. G.A. Askaryan and N.M. Tarasova, JETP Lett. 20, 123-4 (1974).
9. D.E. Lencioni, "Optical Propagation in the Atmosphere", in NATO AGARD Conference Proceedings No. 138, 32-1 (May 1976).

10. J.R. Greig and R.E. Pechacek, NRL MR 3461 (1977)  
(Unpublished).
11. Ya B Zel'dovich and Yu P. Raizer, "Physics of Shock Waves and High Temperature Hydrodynamic Phenomena", Academic Press, New York 1966, Vol. I, p. 188.
12. F. Burhorn and R. Wienecke, Z. Phys. Chem. 215, 269-284 (1960).
13. E.V. Stupochenko, I.P. Stakhanov, E.V. Samuilov, A.S. Pleshanov, I.B. Rozhdestvenskii in "Physical Gas Dynamics" Edtd. A.S. Predvoditelev, Pergamon Press, New York 1961, p. 1-40.
14. R.G. Little and M.B. Kime, "Thin Film Mapping of Electron Accelerators", Simulation Physics, Bedford, Mass. (Unpublished).
15. J.D. Jackson, "Classical Electrodynamics," Wiley, New York, 1962, Chap. 13.
16. W.H. Bennett, Phys. Rev. 45, 890 (1934).
17. E.P. Lee, Phys. Fluids 19, 160 (1976).
18. R.F. Fernsler, A.W. Ali, J.R. Greig, and I.M. Vitkovitsky, NRL-MR 4110, November 1979 (unpublished).
19. L.G.H. Huxley and R.W. Crompton, in "Atomic and Molecular Processes". Edited by D.R. Bates, Academic Press, New York, 1962, Chap. 10.

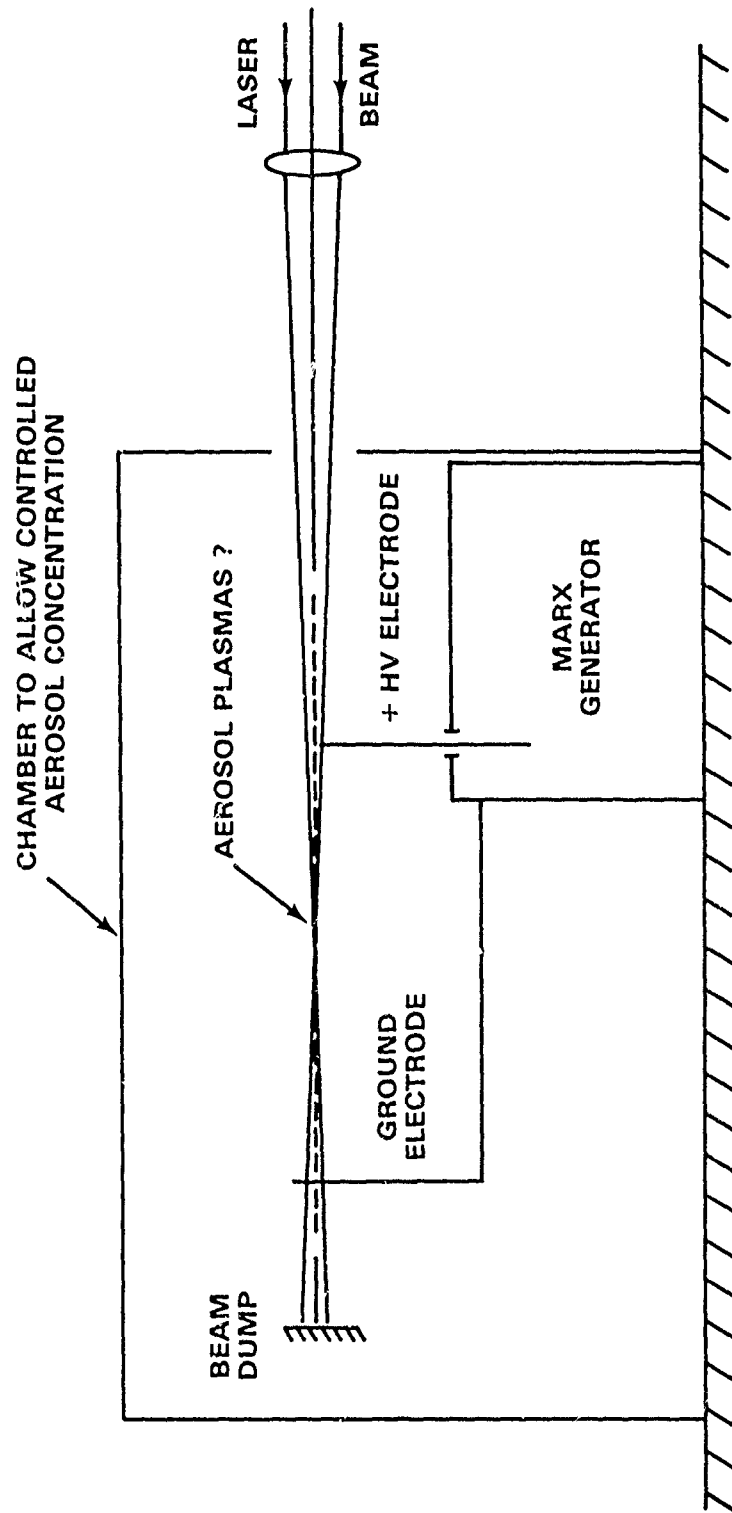


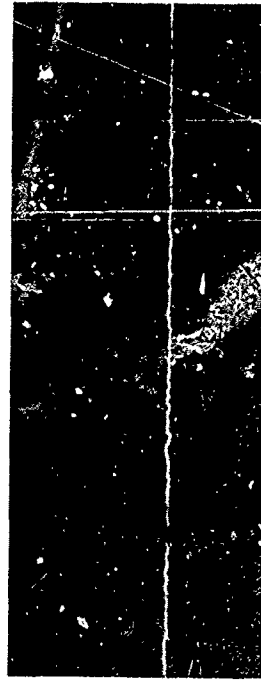
Fig. 1 - The arrangement for creating laser-initiated electric discharge heated channels in the atmosphere



(a)



(b)



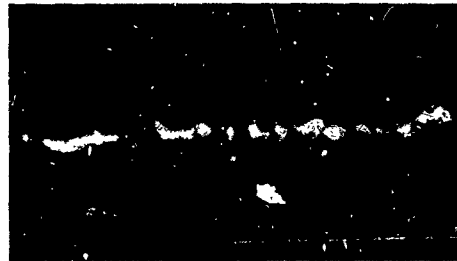
(c)

Fig. 2 - Open shutter photographs of laser designated, electric discharge heated channels in the atmosphere. a) Nd:glass laser + aerosols, b) Laser guided discharge (1m,  $\sigma$  10 kA), c) Laser guided discharge (1m,  $\sigma$  10 kA) photograph shows only 50 cm length. a) and b) were taken at the same lens aperture, c) was taken with reduced aperture.

(a)



(b)



(c)



—| 5 cm

Fig. 3 - Open shutter and Schlieren photographs of laser designated, electric discharge heated channels in the atmosphere. a) Schlieren of laser alone, b) Open shutter of laser guided discharge, c) Schlieren of laser guided discharge. Both a) and c) were taken 31  $\mu$ s after the Nd:glass laser was fired, and in b) and c) the electric discharge was initiated  $\sim$  30  $\mu$ s after the Nd: glass laser.

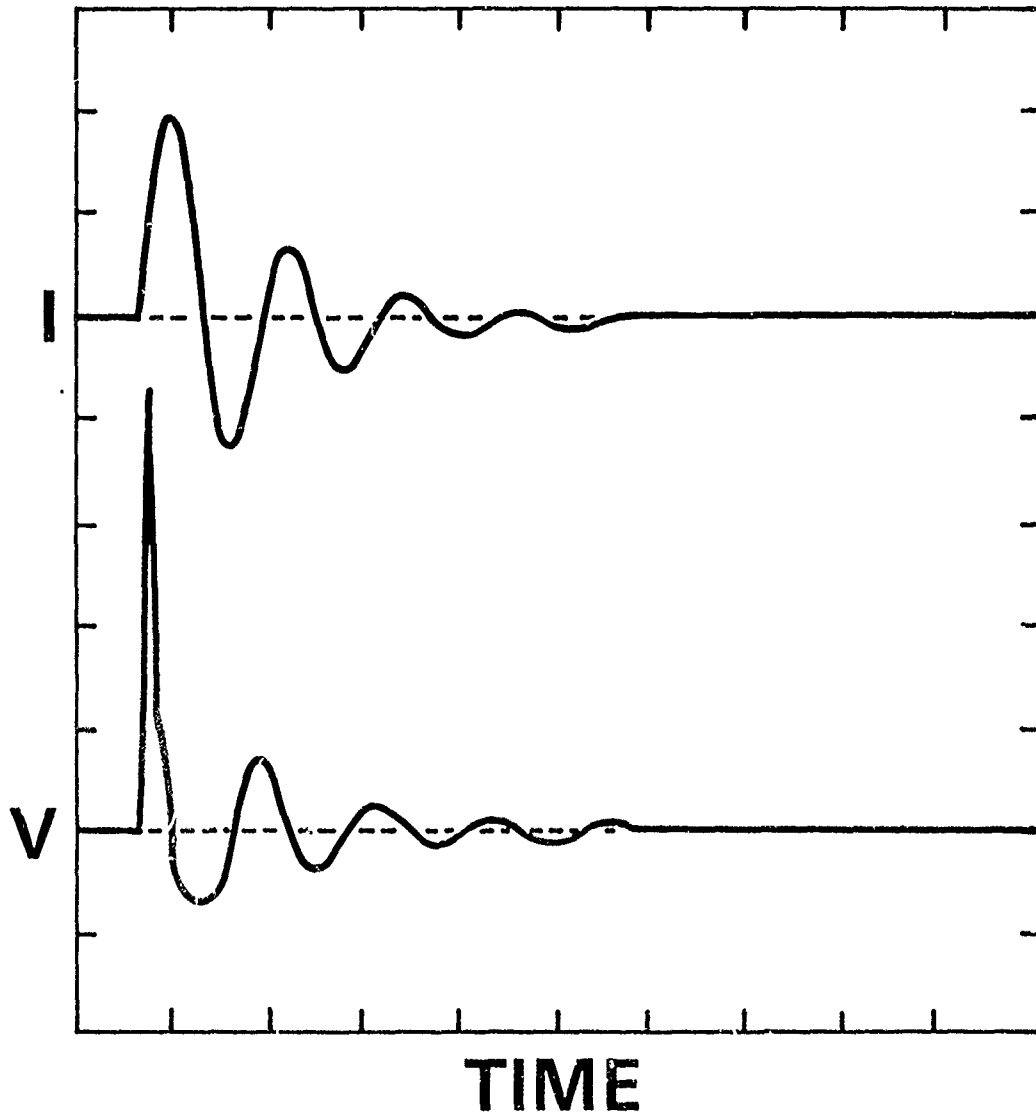


Fig. 4 - Current and voltage traces for a 50 cm long laser guided discharge. The scale for the current (I) is 5.6kA/div, for the voltage (V) 73 kV/div, and for the time 2  $\mu$ s/div.

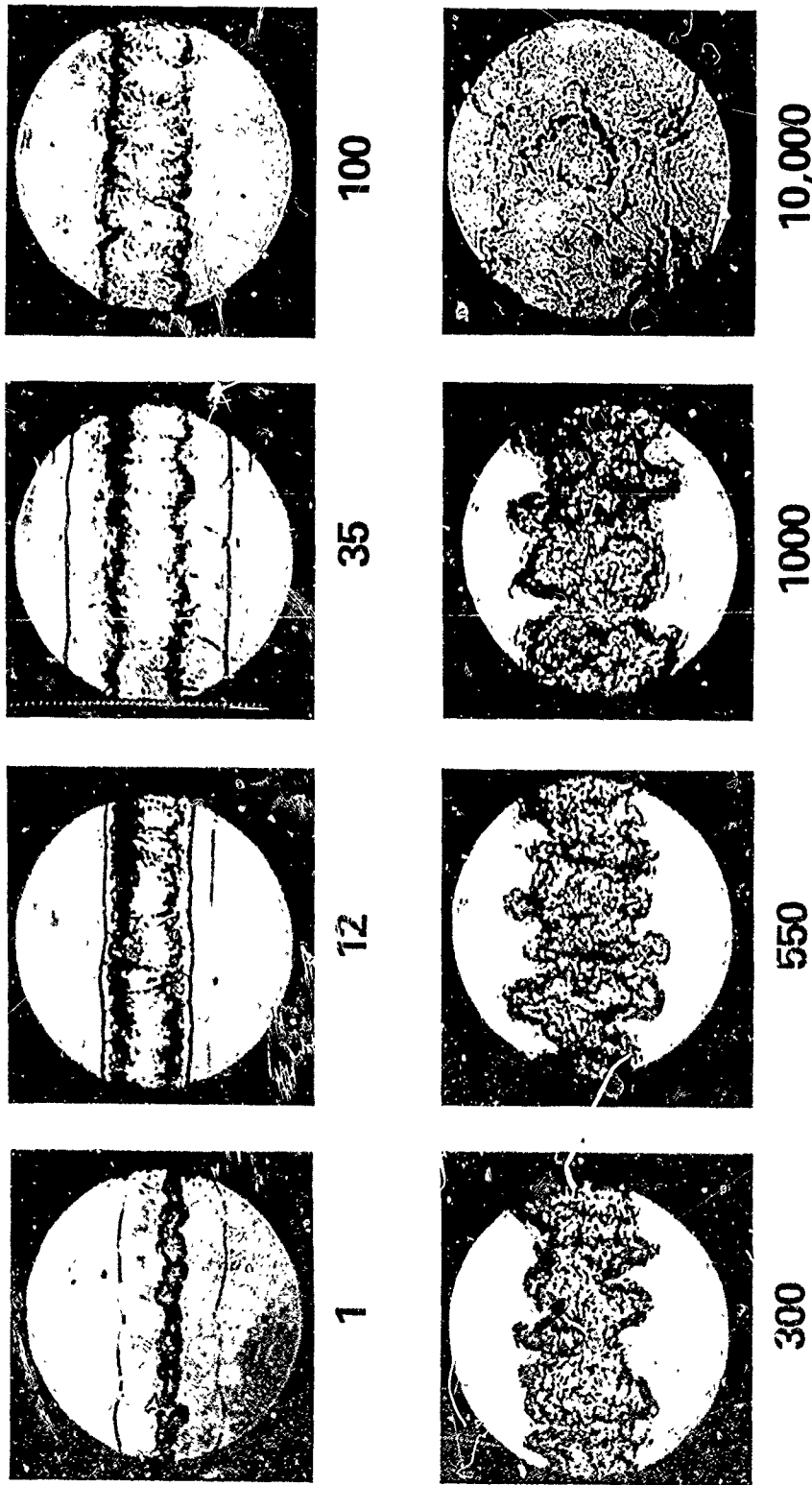
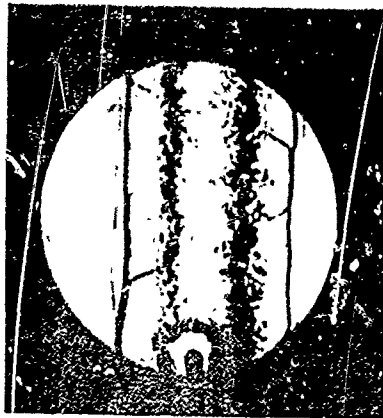
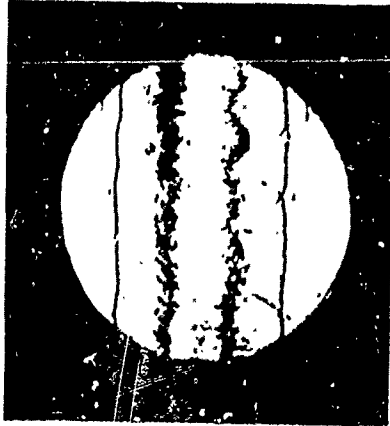


Fig. 5 - Schlieren photographs of laser designated, electric discharge heated channels in the atmosphere. Times are given in microseconds after the initiation of the heating current pulse at which each photograph was taken. Exposure time  $\approx 25 \times 10^{-9}$  sec; wavelength  $\approx 6.9 \times 10^{-5}$  cm; position approximately at center of 100 cm long channel



(a)

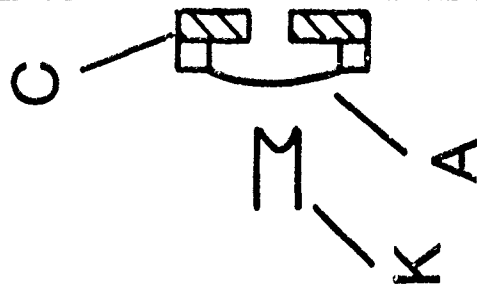


(b)



(c)

Fig. 6 - Schlieren photographs of 100 cm laser designated, electric discharge heated channels in the atmosphere at 30 sec after initiation of the heating current pulse. a) At the high voltage electrode; b) in the center of the channel; and c) at the ground electrode.



100 cm

Fig. 7 - The intense relativistic electron beam propagating in the atmosphere. K is the carbon cathode, A is the titanium anode foil, C is the carbon block. The net beam current at injection was  $I_b \approx 2.2$  kA.

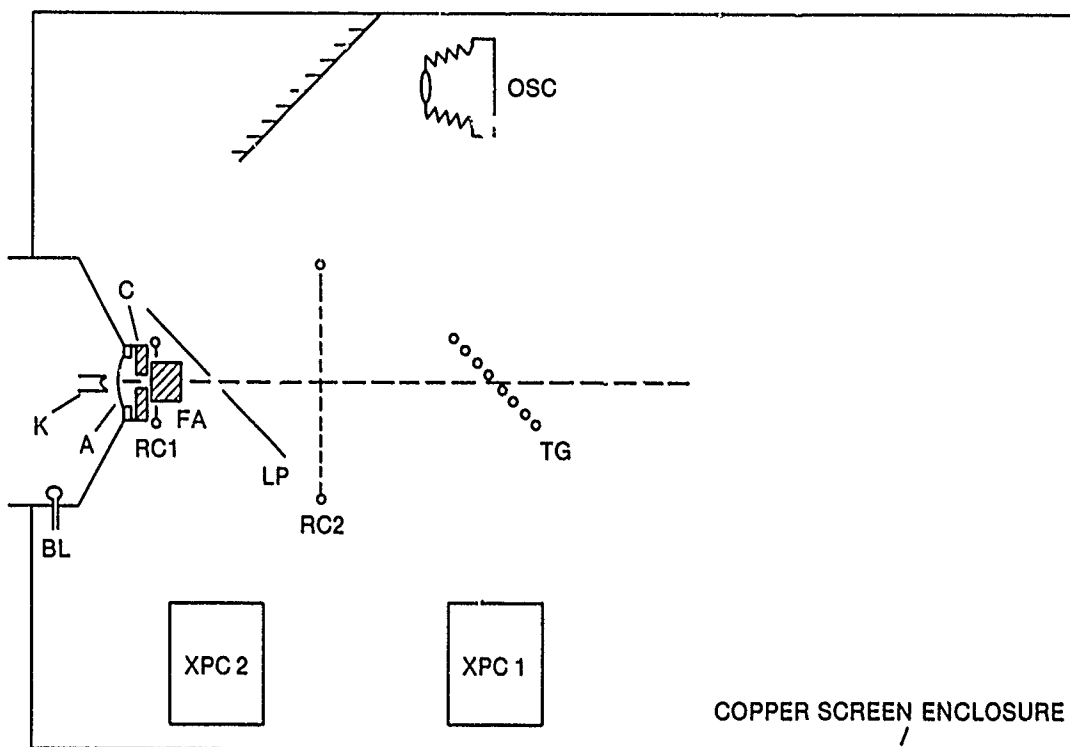
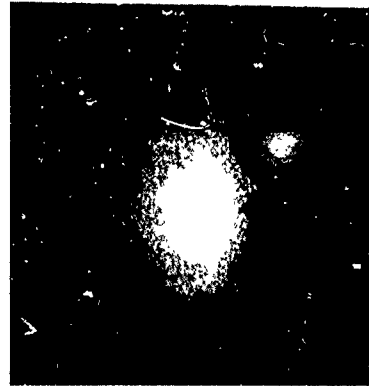
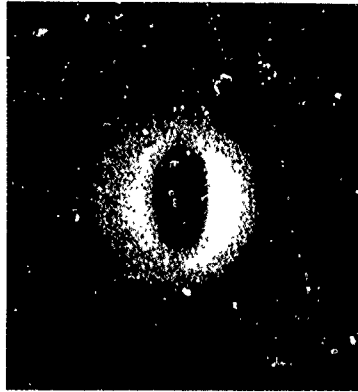


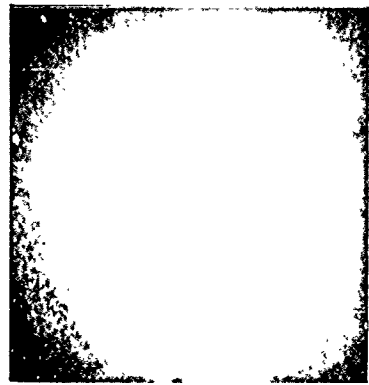
Fig. 8 - A schematic view of the experiment showing the diagnostic systems employed. K - Cathode; A - Titanium anode foil; C - Carbon block; BL - B - dot loop; RC 1 - first Rogowski coil; FA - Foil assembly; LP - Lexan sheet; RC 2 - second Rogowski coil; TG - Tungsten wire grid; XPC 1 and XPC 2 - x-ray pinhole cameras; OSC - Open shutter camera. Note that the whole beam propagation area was enclosed in a copper screened room to reduce electromagnetic pulse radiation. The screened room was approximately 3m x 3m x 5m.

Fig. 9 - Typical results from x-ray pinhole camera photography, XPC 2 on the left and XPC 1 on the right. a) The intense REB injected into the unperturbed atmosphere. b) and c) The REB injected into a hot, reduced density channel at  $\tau = 100 \mu\text{sec}$ . All photographs were taken with the same camera settings, and the frame size shown for XPC 1 represents a vertical dimension of 33 cm at the tungsten grid.

(a)



(b)



(c)

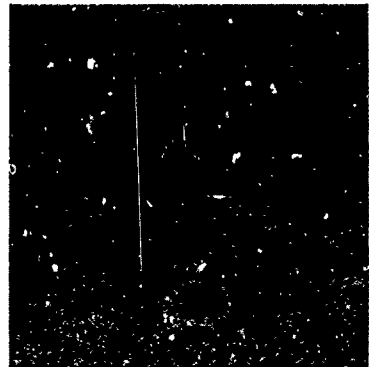
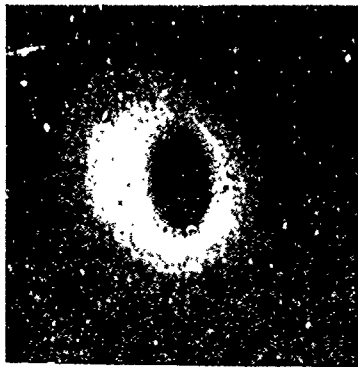
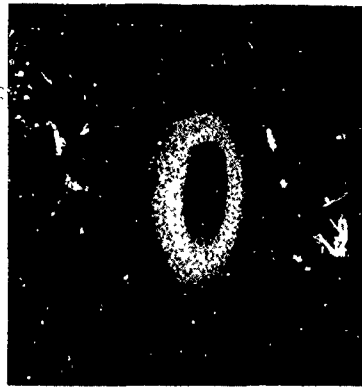
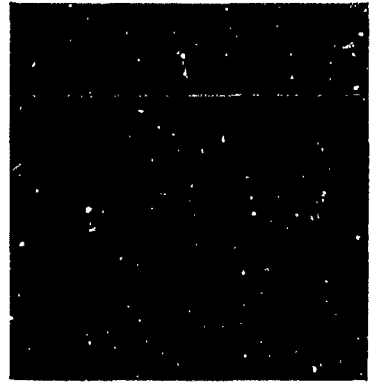
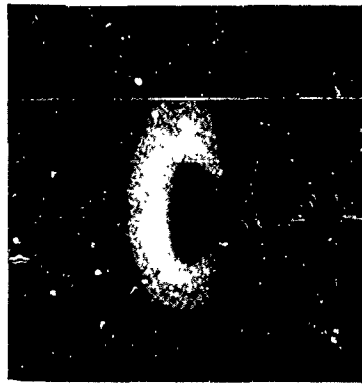


Fig. 10 - Results from x-ray pinhole camera photography, XPC 2 on the left and XPC 1 on the right. a) The REB injected into the unperturbed atmosphere. b) The REB injected into a hot, reduced-density channel at  $\tau = 100 \mu\text{sec}$ . c) The REB injected into a hot, reduced-density channel at  $\tau = 500 \mu\text{sec}$ . All photographs were taken with the same camera settings, and the frame size shown for XPC 1 represents a vertical dimension of 33 cm at the tungsten grid.

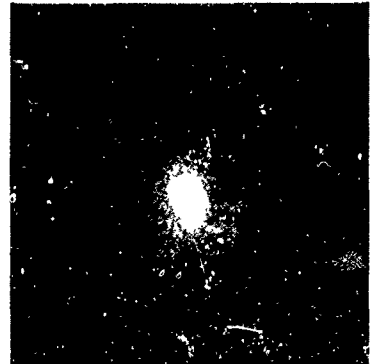
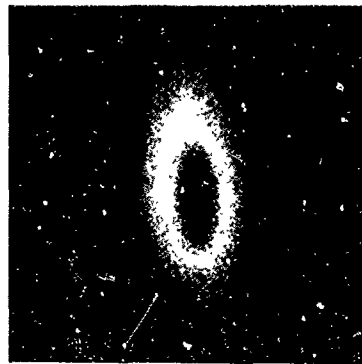
(a)



(b)



(c)



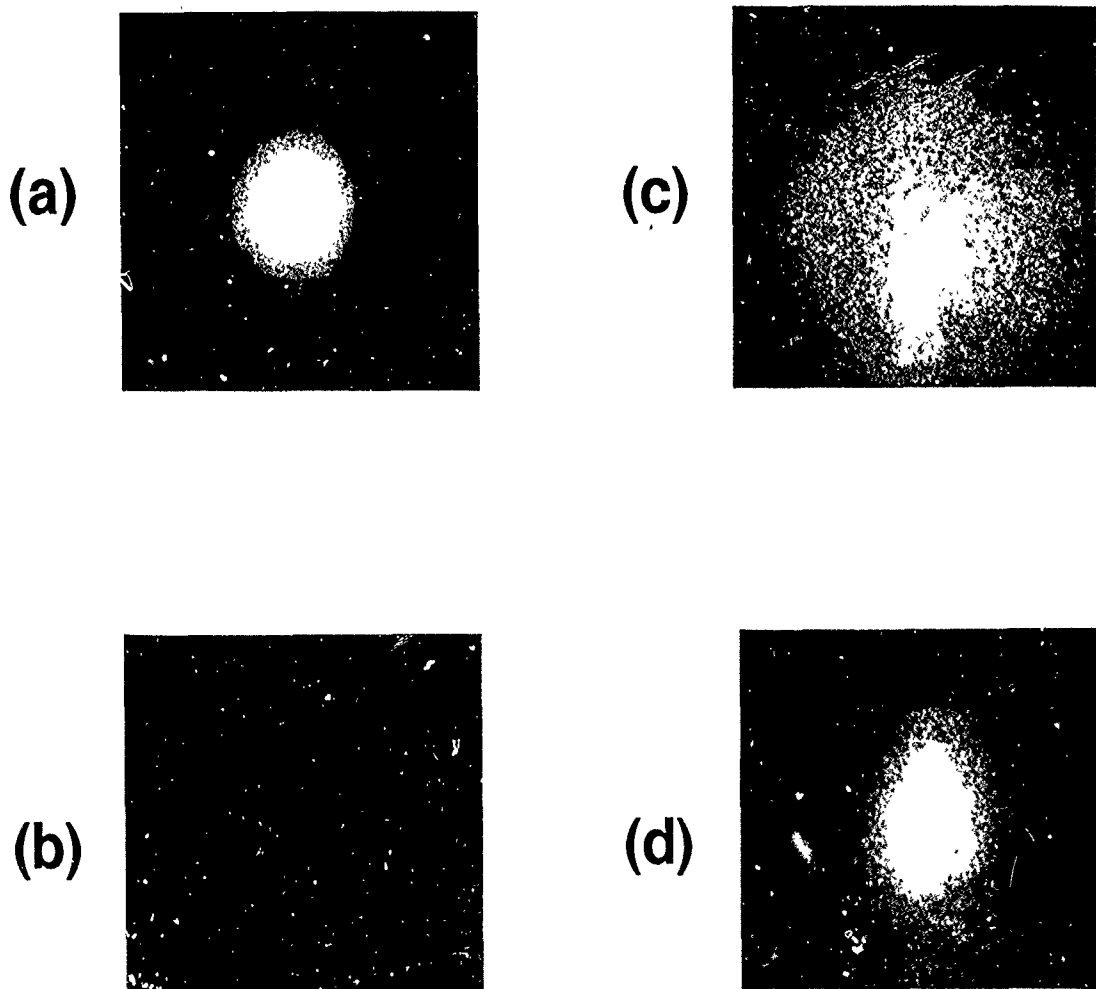


Fig. 11 - X-ray pinhole camera photographs of the Tungsten target. a) The REB injected into the unperturbed atmosphere. b) and c) The REB injected into a hot, reduced-density channel at  $\tau = 100 \mu\text{sec}$ . d) The REB injected into a hot, reduced-density channel at  $\tau = 500 \mu\text{sec}$ . Photographs a) and b) were taken at the same camera setting as those in Fig. 9, photographs c) and d) were taken at the same settings as those in Fig. 10, but for these photographs the Lexan plate (LP in Fig. 8) was removed. The frame size shown represents a vertical dimension of 33 cm at the tungsten grid.

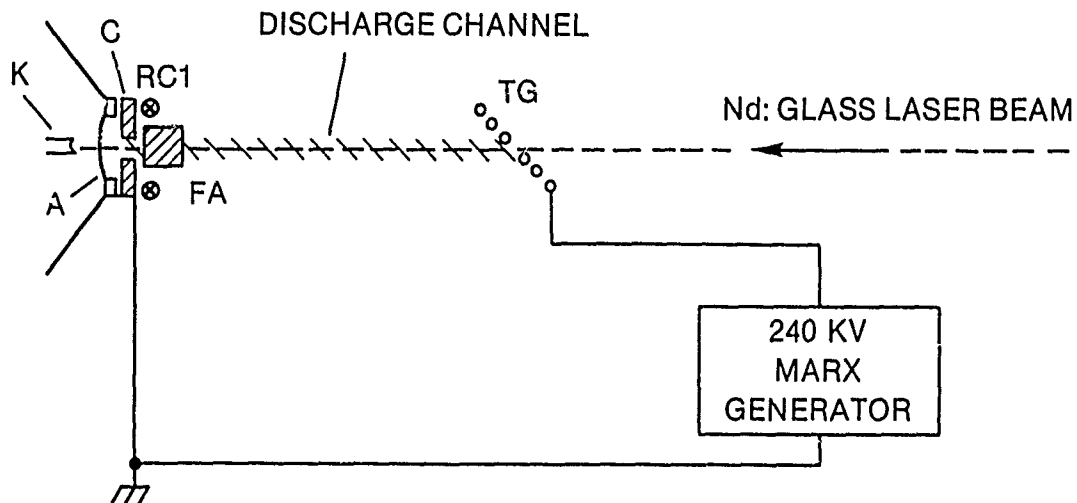


Fig. 12 - A schematic view of the experiment to inject the REB into a preformed channel.

- K - Cathode
- A - Titanium foil anode
- C - Carbon block
- RC 1 - Rogowski coil 1
- FA - Foil assembly
- TG - Tungsten grid

The distance from the Tungsten grid to the carbon block was 50 cm.